Preliminary Investigation on Steel Jacketing Retrofitting of Concrete Bridges Half-Joints

applied sciences

IMPACT FACTOR 2.7

CITESCORE 4.5

Article

Preliminary Investigation on Steel Jacketing Retrofitting of Concrete Bridges Half-Joints

Gabriele Bertagnoli, Mario Ferrara, Luca Giordano and Marzia Malavisi

Special Issue

Existing Bridges: From Inspection to Structural Rehabilitation

Edited by

Prof. Dr. Pier Paolo Rossi and Dr. Nino Spinella

MDPI

https://doi.org/10.3390/app13148181

applied sciences

MDPI

Article

Preliminary Investigation on Steel Jacketing Retrofitting of Concrete Bridges Half-Joints

Gabriele Bertagnoli [1,*], Mario Ferrara [1], Luca Giordano [1] and Marzia Malavisi [2]

[1] Department of Structural, Geotechnical and Building Engineering (DISEG), Politecnico di Torino, 10129 Turin, Italy; mario.ferrara@polito.it (M.F.); luca.giordano@polito.it (L.G.)
[2] Movyon, Autostrade per l'Italia S.p.A., 50013 Limite, Italy; marzia.malavisi@movyon.com
* Correspondence: gabriele.bertagnoli@polito.it; Tel.: +39-3462466367

Abstract: An innovative strengthening system for dapped-end beams is studied numerically and experimentally in this paper. The system is developed for the half-joint regions of bridge beams also commonly called "gerber saddles", but it can be adapted to different scenarios. The strengthening system consists of two steel plates that are clamped on both sides of the webs of the beams by means of bolts. The purpose of the system is to transfer the highest possible amount of shear from the concrete webs to the steel plate elements reducing the resistance demand of the concrete half joint. Shear is transferred by friction from concrete to steel plates. The system is designed to be applied on existing bridges without heavy work interesting the carriageway, therefore reducing the interference with the traffic. Some interesting considerations emerge from the study, including the influence of the flange web connection on the structural behavior and the possible presence of brittle failure mechanisms that are difficult to model numerically using f.e.m. simulations.

Keywords: dapped-end beams; half-joints; bridges; beams; concrete; strengthening; steel jacketing

Citation: Bertagnoli, G.; Ferrara, M.; Giordano, L.; Malavisi, M. Preliminary Investigation on Steel Jacketing Retrofitting of Concrete Bridges Half-Joints. *Appl. Sci.* **2023**, *13*, 8181. https://doi.org/10.3390/app13148181

Academic Editor: Syed Minhaj Saleem Kazmi

Received: 30 April 2023
Revised: 11 July 2023
Accepted: 12 July 2023
Published: 13 July 2023

1. Introduction

In Italy and, in general, in the western part of the world, the largest part of the road and highway network was developed and built between the 1950s and the 1980s. Road structures today show in some cases a marked degradation [1], mostly due to their age, lack of maintenance, and design or construction faults. Reinforced concrete deterioration, such as carbonation, reinforcement corrosion, and spalling of cover can deeply reduce the bearing capacity of bridge structures. Strengthening and retrofitting existing bridges are now among the most important and critical activities within the field of infrastructural engineering. The decreasing safety levels of existing bridges is such an important topic that the Italian Ministry of Infrastructures and Sustainable Mobility published in 2022, in the new Italian guidelines for the safety assessment of existing bridges [2]. An overview of it and a case-study application on an existing bridge can be found in [3–5].

One of the most common examples of deteriorated concrete structures are half-joints, also known as dapped-end beams. These solutions were popular in bridge construction between the 1960s and 1980s because they are simpler than continuous beams (as they are statically determined), even though they share stiffness and section exploitation with them (see Figure 1). The half-joint is a structural detail that has many critical issues and can suffer from very early degradation [6], many times leading to brittle failures. An example of brittle failure of a gerber saddle is given in [7], and a study on the safety level of bridge gerber saddles comparing strut and tie and finite element simulations is also presented in [8]. An interesting study on the effect of reinforcement corrosion on dapped ends is proposed by Di Carlo et al. in 2023 [9].

Numerous studies have been conducted over the years on their structural behavior and strengthening methods, as reported in Section 2.

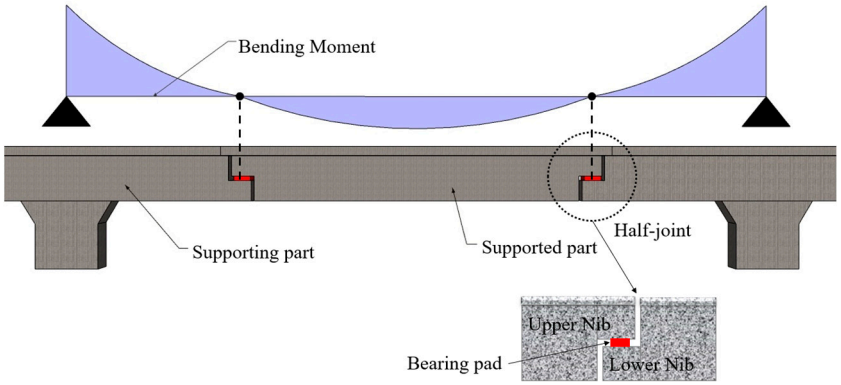

Figure 1. Usual static scheme of a bridge with gerber saddles and half-joint detail.

External prestressing systems are used as a common strengthening procedure for half-joints [10,11]. This procedure necessitates the perforation of the top slab to execute the strengthening work; hence, a prolonged closure of the structure to traffic.

This research focuses on the strengthening of the supporting part of the gerber saddle: the one on the cantilever connected to the pier (therefore subjected to negative bending moment). Many studies are in fact related to the part belonging to the supported beam (subjected to positive bending moment) [12–14], whereas a bibliography is lacking on the negative half. Non-linear numerical modelling and experimental tests on scaled specimens are carried out.

The strengthening system is designed to be as little invasive as possible, with the aim of reducing the closed traffic lanes on the bridge. Four operating phases are individuated:

- web cleaning and application of steel jacketing, Figure 2b;
- supported beam lifting and removal of old bearings, Figure 2c;
- introduction of new bearings connecting steel jacketing elements, Figure 2d;
- re-positioning of a supported beam, Figure 2e.

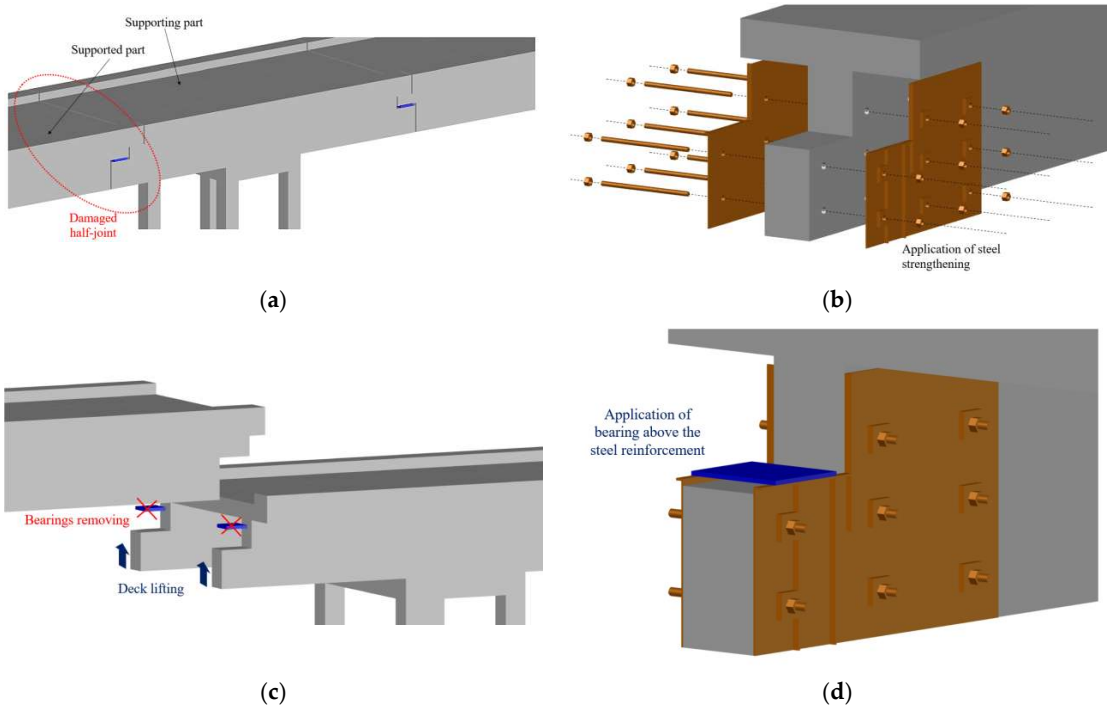

(**a**) (**b**)

(**c**) (**d**)

Figure 2. *Cont.*

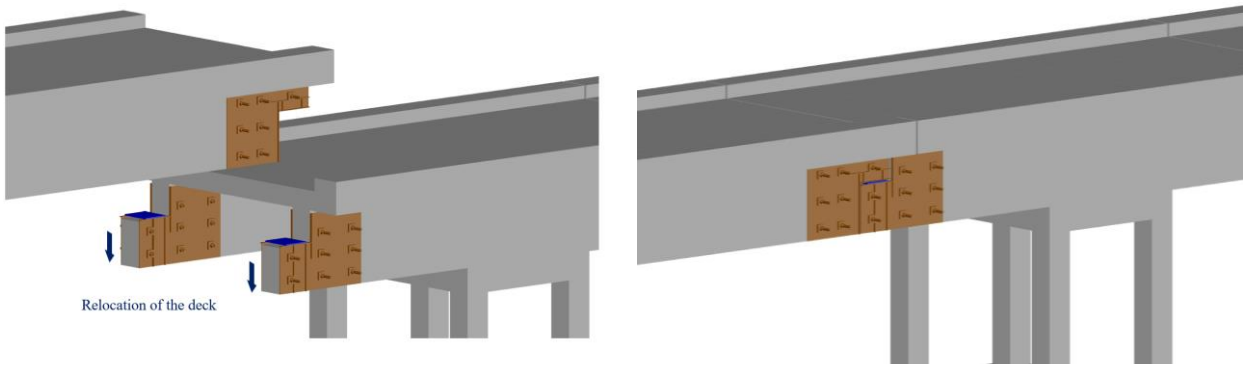

(**e**) (**f**)

Figure 2. Schematic representation of the proposed procedure. (**a**) Original structure. (**b**) Application of steel jacketing. (**c**) Lifting of the deck and removal of old bearings. (**d**) Positioning of new bearings connected to the steel strengthening system. (**e**) Re-positioning of the supported beam. (**f**) Final result.

The only operation that can require the complete closure of the traffic is limited to the lifting phase of the deck and the functionality of the structure is therefore restored, Figure 2f.

The proposed system is applicable, in the present version, only to bridge decks where there is no transverse beam connecting the half joints or where this beam is placed behind the joint.

2. State of the Art

When half-joints started to be used, most studies were aimed at understanding their behavior and the most appropriate calculation methods. In recent times, due to emerging degradation issues, the research became focused on strengthening systems.

One of the first research studies on dapped end beams was performed by Mattock and Chan [15] in 1979, to evaluate the resistance of dapped end beams grounding on the procedure proposed by Mattock in 1976 [16]. It is based on the application of the static theorem of plasticity theory.

In 1983, Liem carried out a new experimental campaign based on the approach proposed by Mattock and Chan [15] but using inclined reinforcement in the discontinuity zone [17]. Over the years, the calculation of discontinuity zones was increasingly performed with Strut and Tie Models (STM). The STM is based on the static theorem (lower limit) of plasticity theory. To date, it is the only method recommended in design standards to calculate discontinuity zones. The first application of STM to the calculation of half-joints was performed by Barton in 1991 [18]. Today the STM proposed by Desnerck in 2018 [19], which can also take into account damage conditions, and the simplified model proposed by Falcon in 2019 [20] are very popular.

In addition to calculation methods, important studies have been conducted on the parameters influencing the strength of dapped end beams, in particular the arrangement of reinforcement in the discontinuity zone [21–23].

In recent years, research on this structural typology has focused mainly on strengthening systems and numerical simulation using finite elements.

The most used strengthening systems can be grouped into two types:

- Fiber Reinforced Polymers (FRP) or Carbon Fiber Reinforced Polymers (CFRP) strengthening systems [12,13,24–28];
- Structural strengthening systems based on external prestressing [14,29].

Strengthening performed with FRP or CFRP shows very high variability in effectiveness. The increase in load-bearing capacity can vary between 10% and 80% and depends on fiber orientation, the geometry of the discontinuity zone, and the arrangement of original

rebar reinforcement in the discontinuity zone. Reinforcements performed with external prestressing are generally more efficient.

Most of the studies focus on strengthening techniques based on the application of composite materials. The main advantage of these methods is that they do not require additional damage to the joint, such as drilling holes during repair phases. On the contrary, external prestressing systems show overall better performance but are more complicated and difficult to install.

3. Research Motivations

Grounding on the state of the art reported in Section 2, the authors decided to investigate a new strengthening system that should be applicable to overcome heavy structural deficiencies, but less invasive than external prestressing introduction.

The idea behind the strengthening system is very simple: two L-shaped steel plates are placed on both sides of the webs of the longitudinal beams in correspondence with the half joint; a transverse prestressing force is applied using (8.8 or 10.9) bolts and threaded rods; shear force pass from the concrete webs to the steel plates thanks to the friction created by the transverse prestressing. In the ideal case, all the force is transferred passing through the steel plates and bypassing the damaged and weak concrete half-joint.

In bridge decks, a top slab is always present to provide support for the carriageway. Therefore, most longitudinal bridge beams are T-shaped or I-shaped if a bottom slab is also present.

The steel plates on the supported beam can be joined together under the bottom of the web creating a U steel jacketing that completely encloses the tensed longitudinal reinforcement placed at the bottom of the web (see Figure 3).

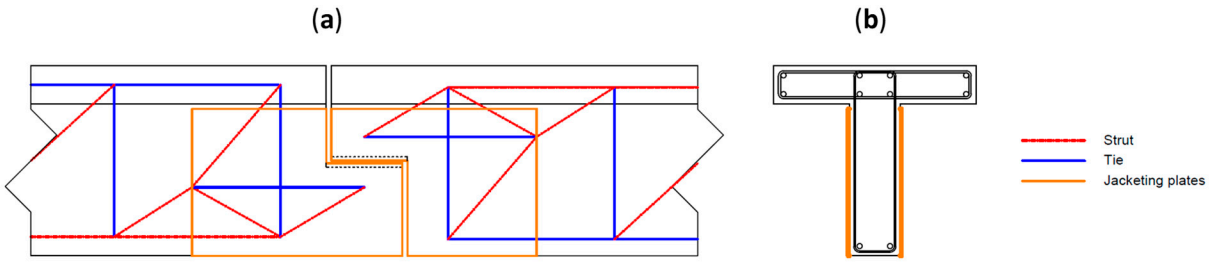

Figure 3. (**a**) Longitudinal view of half joint with jacketing plates and strut and tie system. (**b**) Cross section of typical T-shaped bridge beam.

On the contrary, the tensed chord of the supporting beam is placed inside the top flange and therefore the jacketing steel plates cannot reach it as they do not cross through the top slab (see Figure 3).

Therefore, the two beams work in different conditions from the point of view of the jacketing: an easy one for the supported beam and a difficult one for the supporting one. The research presented in this paper aims to study the resisting mechanisms of the jacketed supporting beam in order to test the system on the most severe side.

All the studies found in the bibliography referred to experimental tests carried out on rectangular cross-section beams working in the static scheme of the supported beam. Therefore, no interaction with the flanges has been assessed before in the literature, especially with regard to strengthening a T beam where the tensed chord is in the flange of the T.

The presented study proposes the following novelties: testing performed on the supporting part of a gerber saddle (subject to negative moment); a strengthening system for heavy damage, but less invasive than strengthening systems with post-tensioning; and experimentation on a beam with a T-section to consider the effects between the casting joint between beam and slab.

4. Description of the Experimental Campaign

An experimental campaign on two beams realised in 1/3 scale was designed by the authors and it is described in the following paragraphs.

4.1. Description of the Dapped-End Beams

Two dapped-end beams were designed with the same geometry as shown in Figure 4. Both are T beams, 75 cm deep with an 80 cm wide flange and a total length of 4.9 m.

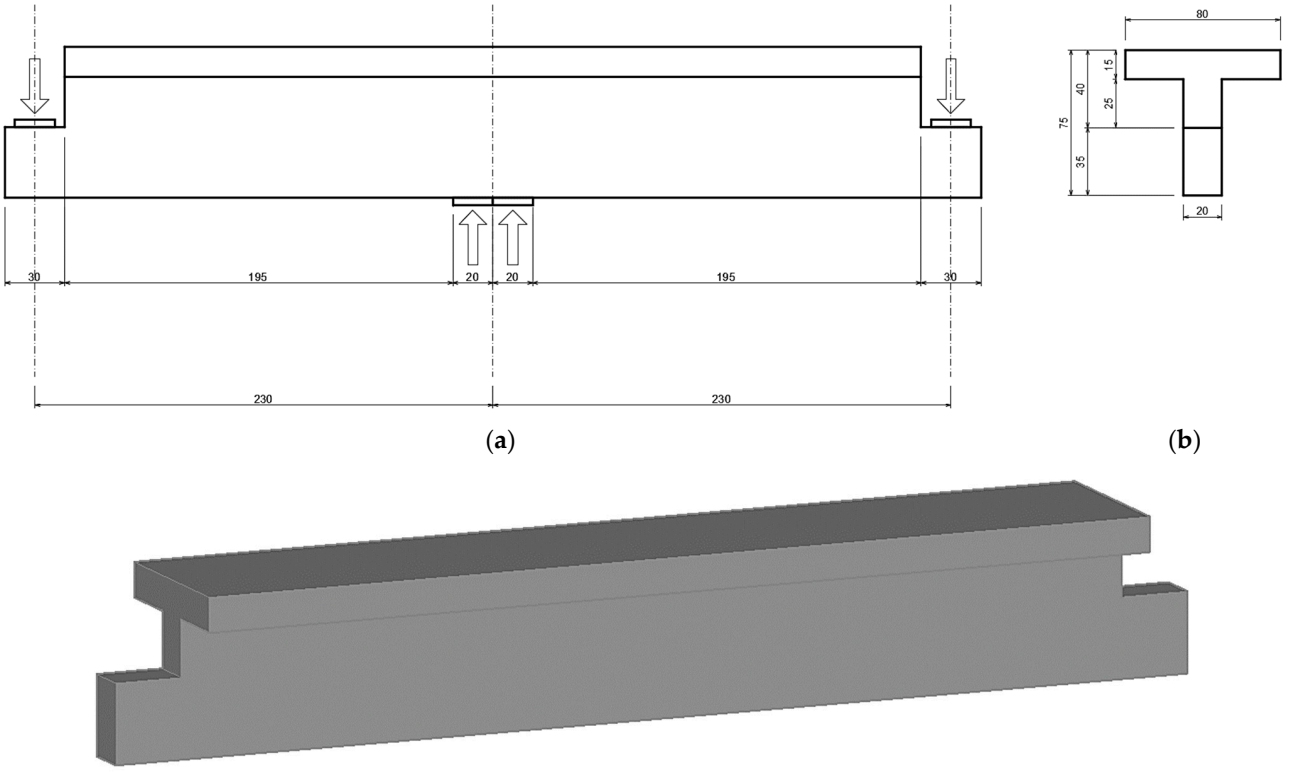

Figure 4. The geometry of beams. Dimensions in cm. (**a**) Longitudinal view. (**b**) Cross section. (**c**) 3D view.

Each specimen represents one of the longitudinal beams of the part of the deck of the bridge rigidly connected on top of the pier: the so-called hammer. The pier provides the central support (as shown in Figure 4) and the drop-in spans load the hammer's half joints on the two sides. Each specimen, being 1/3 scale, represents a real cantilever span of 6.6 m realised with a 2.25 m deep beam. The specimens are tested upside down in the laboratory, being vertically loaded at the center by a hydraulic jack and simply restrained on both sides on the half-joints. This choice increases the stability of the test. In fact, an unstable configuration during testing may arise having only one central support and loading the two dapped ends. On the contrary, a single central jack is more controllable and the load that in reality is applied by the drop in span in the dapped ends is simulated by means of the bearings' reactions in the lab.

Both specimens are designed to reach local failure within or close to the half-joint avoiding classical bending or shear failure of the current T section.

One specimen is realised with orthogonal reinforcement in the dapped end and the other with an inclined one. Details on the arrangement of reinforcement are shown in Figures 5 and 6. The two different reinforcement arrangements are designed to simulate the two common arrangements in real bridge beams.

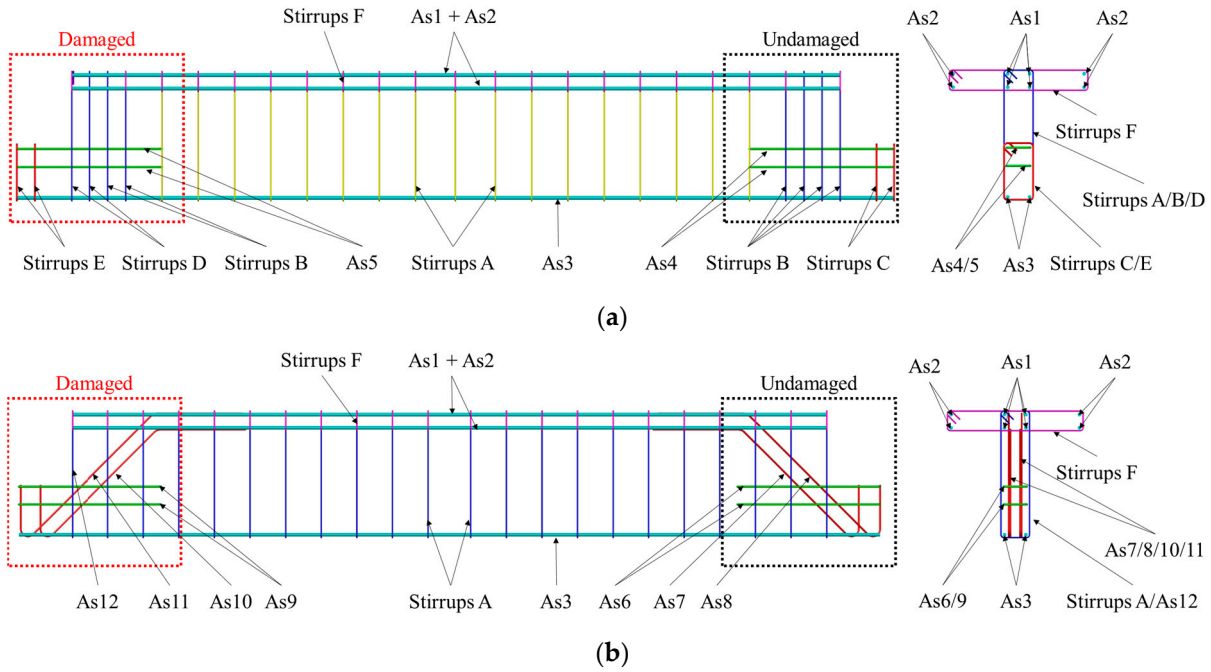

Figure 5. Reinforcement arrangement in the discontinuity zone. (**a**) Orthogonal layout. (**b**) Inclined layout.

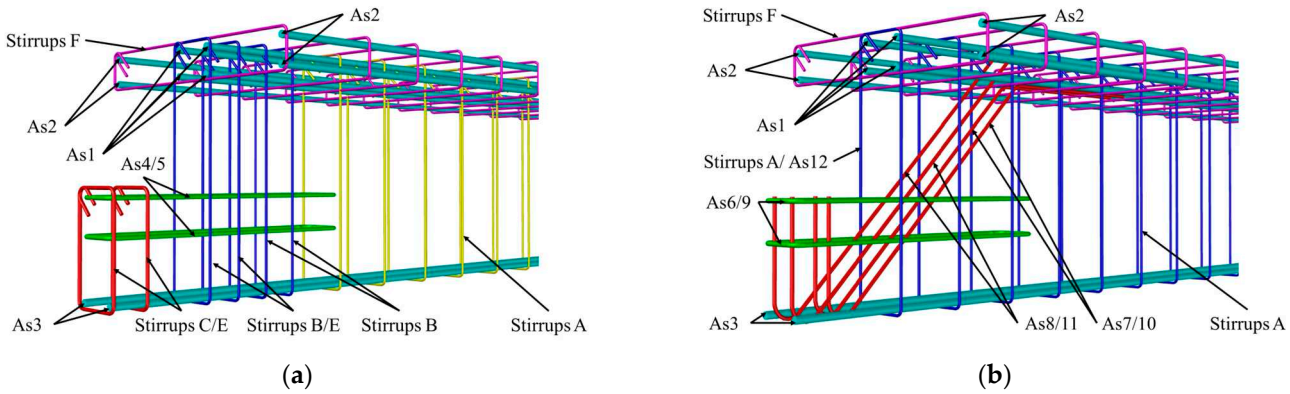

Figure 6. Detail of the reinforcement arrangement. (**a**) Orthogonal layout. (**b**) Inclined layout.

The beams were designed with a strut and tie model (STM) according to [30]. The STMs adopted are shown in Figure 7. In both beams, the left half-joint was created with correct design reinforcement and the right one with reduced reinforcement to simulate steel bars corrosion. The side with reduced reinforcement was afterwards strengthened with steel plates. The choice of using rebars with smaller diameters to simulate deterioration is due to the boundary conditions of this experimental campaign. The research program was part of a funding competition between universities and the funding institution gave a four months time window to accomplish the research. Accelerated corrosion processes, may need from 30 days for very simple specimens [31] up to 70 days for complex specimens as in the present case [32]. Therefore, even accelerated corrosion was too time demanding to respect the time limit.

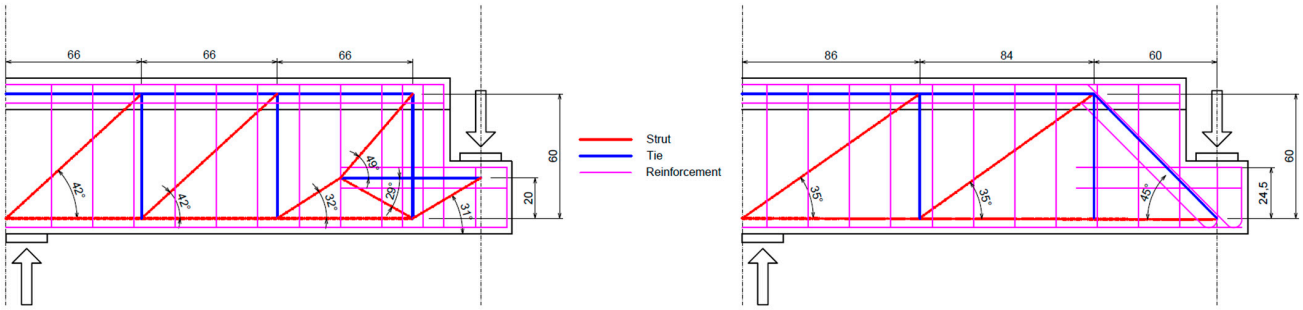

(**a**) (**b**)

Figure 7. Adopted STM. (**a**) Orthogonal reinforcement. (**b**) Inclined reinforcement.

Reinforcement details are shown in Figures 5 and 6 and Table 1.

Table 1. Reinforcements detail.

Reinforcement Name	Description
As1	4Φ20 L = 484 cm
As2	4Φ20 L = 484 cm
As3	2Φ20 L = 484 cm
As4	2Φ12 L = 196 cm
As5	2Φ8 L = 196 cm
As6	2Φ8 L = 196 cm
As7	2Φ8 L = 167 cm
As8	2Φ10 L = 180 cm
As9	2Φ6 L = 196 cm
As10	2Φ6 L = 167 cm
As11	2Φ6 L = 180 cm
As12	1Φ6 L = 184 cm
Stirrups A	Φ8/20 L = 184 cm
Stirrups B	Φ10/10 L = 184 cm
Stirrups C	2Φ10 L = 104 cm
Stirrups D	2Φ6/10 L = 184 cm
Stirrups E	2Φ6 L = 104 cm
Stirrups F	Φ8/20 L = 184 cm

The following reinforcement reductions were applied in the damaged dapped end of the beam with orthogonal reinforcement:

- **Horizontal reinforcement in the dapped end**. From 2Φ12 (As4) in the sound side to 2Φ8 (As5) in the damaged one: −56%.
- **Vertical reinforcement in the dapped end**. From 4Φ10/10 (Stirrups B) + 2Φ10 (Stirrups C) in the sound side to 2Φ10/10 (Stirrups B) + 2Φ6/10 (Stirrups D) + 2Φ6 (Stirrups E) in the damaged one: −43%.

The following reinforcement reductions were applied in the damaged dapped end of the beam with inclined reinforcement:

- **Horizontal reinforcement in the dapped end**. From 2Φ8 (As6) in the sound side to 2Φ6 (As9) in the damaged one: −44%.
- **Vertical reinforcement in the dapped end**. From 3Φ8/20 (Stirrups A) in the sound side to 2Φ8/20 (Stirrups A) + 1Φ6 (As12) in the damaged one: −15%.
- **Inclined reinforcement in the dapped end**. From 2Φ8 (As7) + 2Φ10 (As8) in the sound side to 2Φ6 (As10) + 2Φ6 (As11) in the damaged one: −56%.

The resistances of the half joint given in Table 2 are obtained according to the reinforcement arrangement shown in Figures 5 and 6 and using the STM shown in Figure 7.

Table 2. Ultimate load according to STM.

Beam Type	Dapped-End Status	Failure STM Load [kN]
Orthogonal reinforcement	Sound	150
	Damaged	65
Inclined reinforcement	Sound	160
	Damaged	70

Both sound and damaged beams are designed in order to reach collapse in the half joint in the compressed concrete strut after yielding the main reinforcement of the half joint.

In the beam with orthogonal reinforcement, collapse occurs after the yielding of horizontal reinforcement As4/5. The strength of the concrete strut inclined of 31° (see Figure 7a) is about 90% greater than the one corresponding to the yielding of reinforcement As4/5.

In the beam with inclined reinforcement, collapse occurs after yielding the inclined As7/10, As8/11, and horizontal As6/9 reinforcement. The strength of the first horizontal concrete strut is about 120% greater than the one corresponding to the yielding of reinforcement.

The authors decided to design both half joints respecting ductility and reaching yielding before concrete failure. The failure load of the damaged end is, respectively, 57% and 56% less than the sound one for the beam with orthogonal reinforcement and for the beam with inclined reinforcement arrangement.

4.2. Design and Detail of Steel Jacketing

The steel jacketing was designed to restore 100% of the strength of the damaged dapped end of each specimen. The resisting model of the strengthening system is the same as a slip-resistant connection between two steel members. In fact, the strengthening system must be able to carry the ultimate load of the undamaged dapped end without slipping at the interface with the web surface. For this reason, it is calculated according to [33] as follows:

$$F_{s,Rd} = \frac{k_s \cdot n \cdot \mu}{\gamma_{M3}} \cdot F_{p,C} \quad (1)$$

where $F_{s,Rd}$ is the design slip resistance of a single preloaded bolt; k_s is a coefficient that depends on the type of hole, here considered equal to 1; n is the number of sliding surfaces, in this case, equals to 2; γ_{M3} is a partial safety factor, considered equal to 1 to calculate mean resistance; $F_{p,C}$ is the preload force of the bolts equal to $0.70 \cdot f_{ub} \cdot A_s$, where f_{ub} is the ultimate strength of the bolt and A_s is the cross-section.

M20 class 8.8 bolts are used. Each bolt is pre-loaded with a force of 137 kN. Considering a friction coefficient between concrete and steel $\mu = 0.3$, the slip resistance of the single bolt is $F_{s,Rd} = 75$ kN. With the bolt arrangement shown in Figure 8, a maximum vertical load of 240 kN can be applied to each couple of steel plates, jacketing the web.

The resistance of the slip-resistant connection between concrete web and steel plates (240 kN) is about 60% higher than the resistance obtained for the sound-dapped ends using the strut and tie method (150 ÷ 160 kN). This choice was conducted because strut and tie models generally underestimate the ultimate load (solution on the safe side) and it is easy to find real laboratory resistances that are 20% to 30% higher than the one supposed using STM. On the contrary, the friction coefficient to be applied to the interface between steel and concrete was unknown as the surface was not prepared and, therefore, irregular.

The authors were expecting a real slip resistance lower than 240 kN and a sound saddle resistance higher than 160 kN. The difference between these values was intended to obtain a fair margin of safety to avoid slipping on the interface.

The resistance of the steel plates was calculated in order to be able to carry the saddle load without superposing to the STM mechanism. Therefore, no sum-up was taken into account. Steel plates are by far stiffer than cracked concrete, therefore they work before the STM mechanism can rise. The concrete under the plates was completely uncracked at the end of the test showing that the steel jacketing was carrying most of the load.

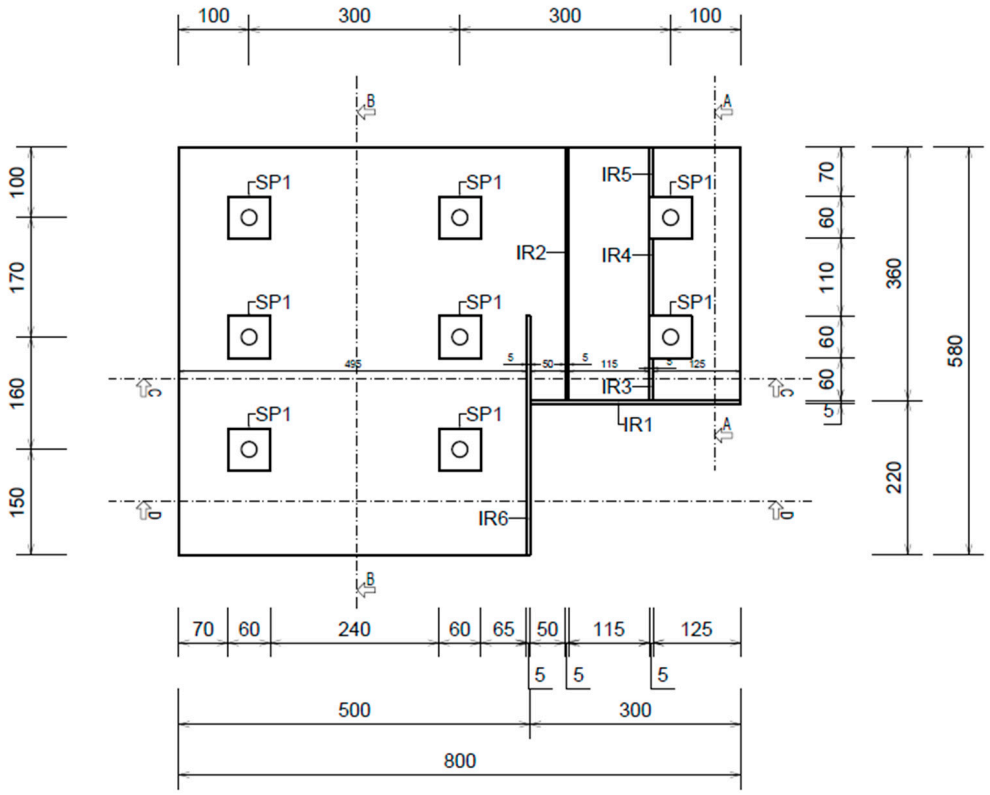

Figure 8. The geometry of the steel plates.

The geometry of the steel strengthening system is shown in Figure 8. The base steel plate is 5 mm thick, its extension inside the beam depends on the extension of the damaged area; in fact, it extends until it is firmly anchored within an area of the beam whit sound shear reinforcement, as can be seen in Figure 9. SP1 elements are squared solid steel 15 mm thick with a side of 60 mm and have the function of diffusing the preload force of the bolt to avoid local failure of concrete under high compression. IR1, IR2, IR3, IR4, IR5, and IR6 elements are 5 mm thick and 15 mm deep. Their function is to avoid instability of the steel plate in the area where the half-joint load is applied directly to it.

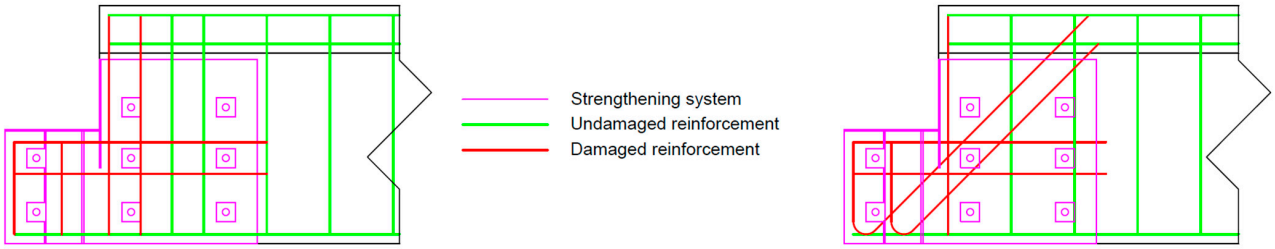

(**a**) (**b**)

Figure 9. Positioning of steel plates and interferences of transverse threaded bars with web reinforcement. (**a**) Dapped end with orthogonal reinforcement. (**b**) Dapped end with inclined reinforcement.

5. Description of the Laboratory Test and the Numerical Simulations

The laboratory tests performed on the two specimens and the nonlinear numerical model that is used to simulate the experimental tests are described in this section.

5.1. Laboratory Tests

The two dapped-end beams were tested according to the static scheme shown in Figure 10a,b. The bearing capacity of the damaged and reinforced end was intended to be similar to the sound one. Therefore, failure was expected on one of the two sides, more probably on the damaged one if some resisting mechanism of the jacketing system was overestimated.

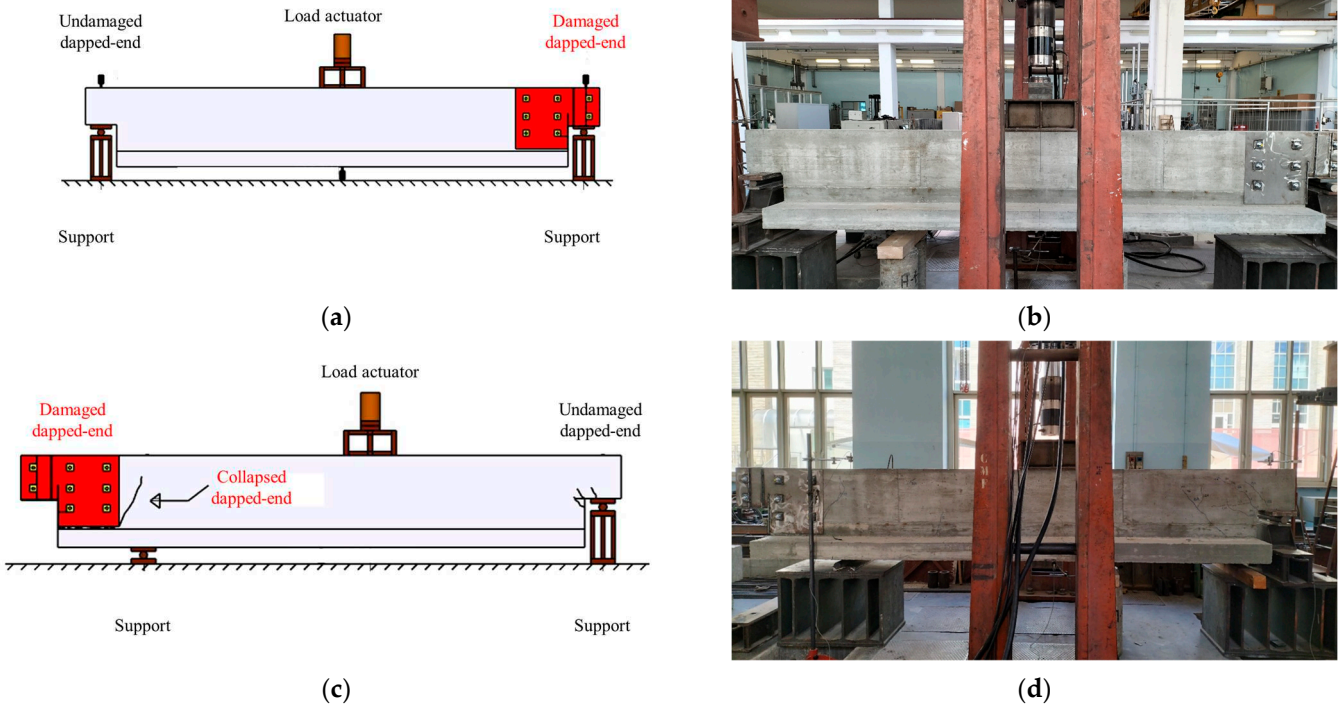

Figure 10. Static schemes of the dapped-end beams during the test. (**a**) Scheme 1. (**b**) Real configuration of Scheme 1. (**c**) Scheme 2. (**d**) Real configuration of Scheme 2.

When one of the two ends collapses, if the other side is not broken, the static scheme can be changed to scheme 2, as shown in Figure 10c,d to load until collapse the other end.

The test was performed in displacement control, imposing a displacement rate of one millimeter per minute.

Tests of the Materials Used to Build the Beams

Experimental tests were carried out on the materials used for the construction of the two dapped-end beams. The following specimens were tested:

- **Concrete:**
  - 6 concrete cubes (150 mm side) were taken from the batch used for the casting of the flange of the two dapped-end beams (1st casting phase).
  - 6 concrete cubes (150 mm side) were taken from the batch used for the casting of the web of the beams (2nd casting phase).
- **Steel**: 3 reinforcement bars of 8 mm diameter and 3 bars of 10 mm diameter.

Tests on concrete cubes provided an average cubic concrete strength of 29.0 MPa for flanges and 29.6 MPa for webs; being the flange completely tensed in the test, its slightly lower compressive strength is not a problem. The results of the tests on rebars are shown in Figure 11; highly ductile behavior is observed, with an average yield stress of 530 MPa and ultimate strain greater than 10%. These mean material characteristics are used in nonlinear numerical models.

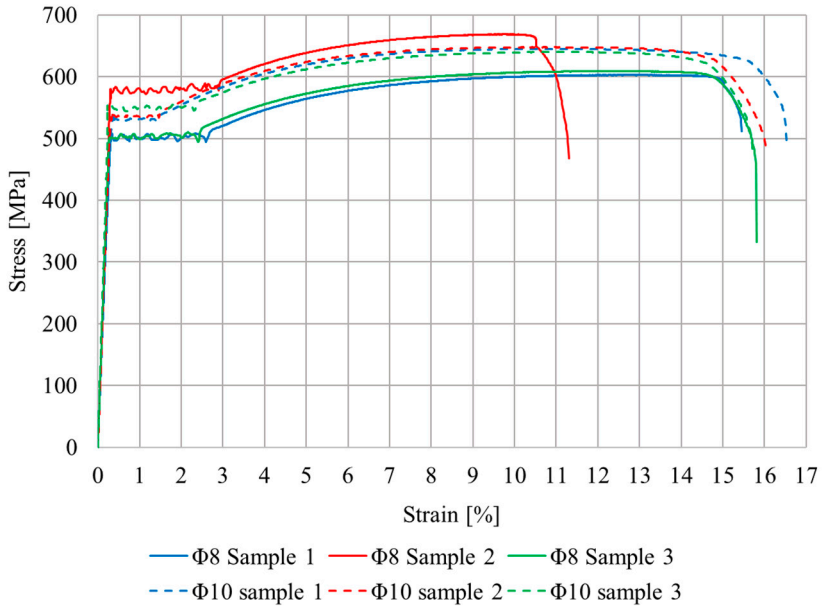

Figure 11. Stress-strain relationship of reinforcement specimens from laboratory tests.

5.2. Nonlinear Numerical Model

The laboratory tests are simulated with a nonlinear f.e.m. model created with DIANA FEA software version 10.4 [34,35]. 3D solid (brick) elements with 20 nodes (Figure 12a) are used for modelling the concrete bodies. Reinforcements are modelled with bar-embedded elements (Figure 12b) in the hypothesis of a full bond between concrete and steel.

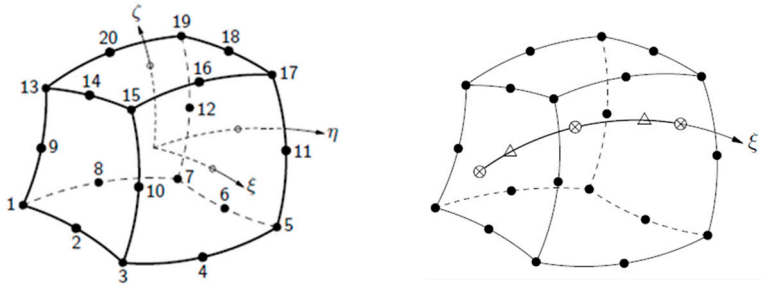

(**a**) (**b**)

Figure 12. Elements used for nonlinear 3D modelling [35]. (**a**) A 20 nodes brick element. (**b**) Embedded bar element.

Brick elements of 30 mm side are used for the concrete parts not in contact with the jacketing plates (Figure 13a), whereas the bricks in contact with the steel plates have a maximum side size of 15 mm (Figure 13b). The mesh dimensions are chosen in order to obtain numerical results not dependent on the mesh size. A Coulomb attritive interface is modeled between steel jacketing plates and concrete. The rebar layout is shown in Figure 14. The supports and loading plates are modeled by means of elastic steel elements to ensure adequate stress distribution and realistic stress concentration in the concrete elements. The interface between support plates and concrete is also modeled with a Coulomb attritive surface. The support plates have plan dimensions of 20 × 20 cm and a thickness of 4 cm. The load plate has plan dimensions of 20 × 40 cm and a thickness of 4 cm. The support plates are constrained in their midline with a hinge (on one side) and a roller (on the other side).

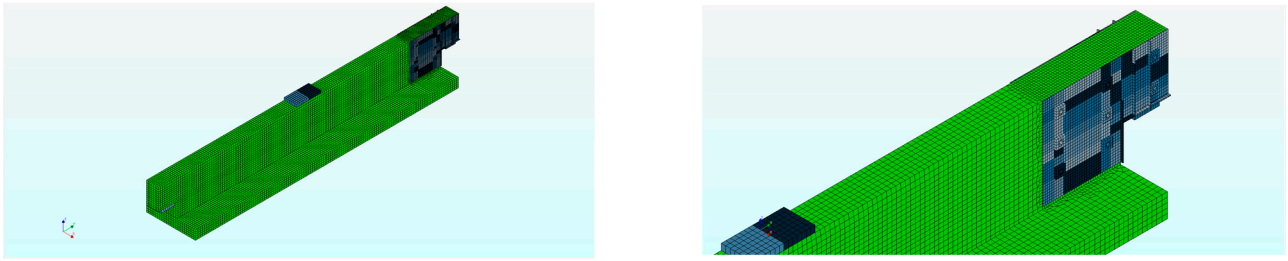

(**a**) (**b**)

Figure 13. Geometry modelling. (**a**) Full view (**b**) Detail of the damaged dapped end.

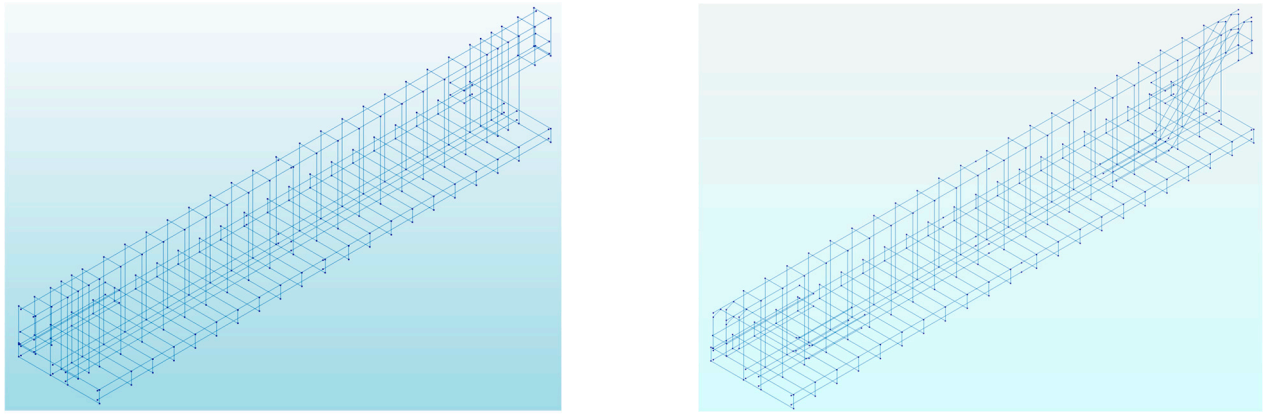

(**a**) (**b**)

Figure 14. The rebars layout. (**a**) Beam with orthogonal reinforcement in the dapped end (**b**) beam with inclined reinforcement in the dapped end.

A Smeared Cracking model is used for concrete [36] with a constitutive law based on the total strain crack model, which in DIANA FEA grounds on the Modified Compression Field Theory [37] extending it to three-dimensional problems following Selby & Vecchio [38]. A linear-ultimate crack strain model is used in tension, with a linear tension softening branch after reaching peak tensile strength (Figure 15a). The stress-strain relationship for concrete in compression is based on EN 1992-1-1 [30] (Figure 15b). The reduction of compressive strength due to lateral cracking is based on the model proposed in [39]. A confinement model based on the proposal by Vecchio & Collins [40] is adopted, and a constant shear retention factor $\beta = 0.2$ is used to describe shear stiffness after cracking.

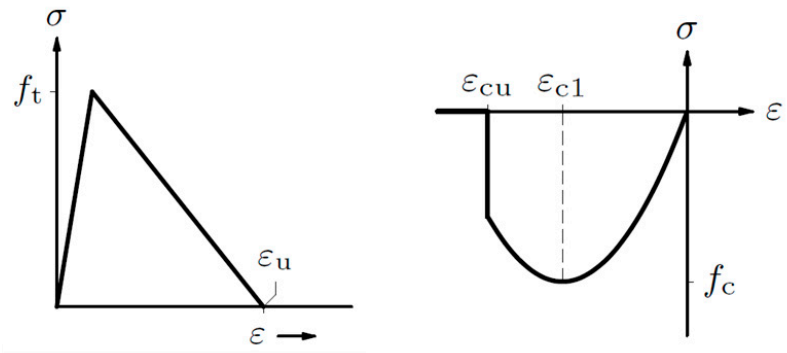

(**a**) (**b**)

Figure 15. Stress-strain relationship for concrete [41]. (**a**) Tension (**b**) Compression.

Elastic-plastic stress-strain relationship with linear hardening is used for reinforcement. Yield strength is 500 MPa, whereas ultimate strength is 550 MPa. An ultimate strain of 10% is chosen.

Jack load is applied with increments of 8 kN per step. The Newton-Raphson integration method is used for reaching convergence.

6. Proposal of a Block Tearing Failure Mechanism

The authors propose an application of the lower bound solution for a plastic approach to manually calculate the failure loads of the beams. A "block tearing" failure mechanism is hypothesised, as shown in Figure 16. The motivation for this model being proposed is because of the brittle fracture that occurred during the laboratory tests, which can be seen in Section 7. This mechanism is used to calculate both the sound and the strengthened end of the beams. The results for the undamaged side have the only purpose of comparison with the other results. For the undamaged side of the gerber saddle, the ultimate load is given by STM being smaller than the block tearing one. For the damaged and strengthened part, the strengthening system was designed to remain in the elastic field, the mechanical properties of the steel of the strengthening system were not taken into account in the block tearing mechanism, but it only influences the assumed collapse surface, thus only at the geometric level and not at the mechanical level.

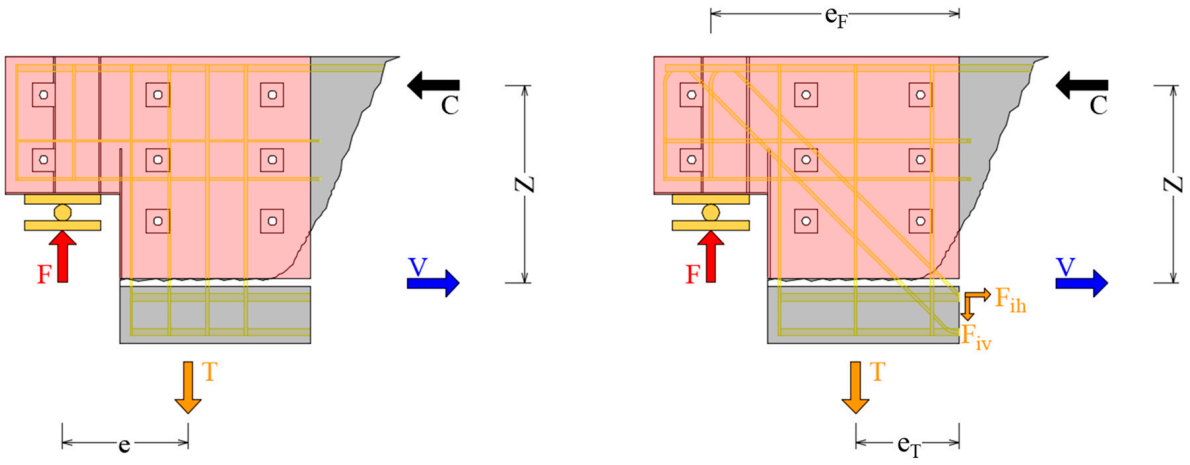

Figure 16. Block tearing failure mechanism for orthogonal (**a**) and inclined (**b**) reinforcement.

A two-side failure surface is considered: the first side is horizontal and it is located at the interface between the web and flange from the free side of the half joint to the end of the steel plate (50 cm long); the second side is vertical and it runs along the vertical side of the steel plate.

6.1. Model for Orthogonal Reinforcement

In the case of orthogonal reinforcement, see Figure 16a, the only forces that are supposed to act on the jacketed block are:

- F Vertical force applied on the half joint;
- T Hanging force in the stirrups;
- C Force in the compressed chord;
- V Shear friction resistance.

Horizontal equilibrium needs $V = C$ and vertical one needs $F = T$.

Vertical stirrups should at least be able to carry the vertical force F, but if their section is bigger than the one needed to carry F, they can provide additional resistance in the shear friction model according to clause 6.2.5 of EN1992-1-1 [30] presented below:

$$V = (c \cdot f_{ct} + \mu \cdot \rho \cdot \sigma_{av}) A_{cj} \quad (2)$$

where the cross-section of the joint A_{cj} is the length of the steel plate multiplied by the web thickness $A_{cj} = 500 \times 200$ mm.

Therefore Equation (2) can be rewritten as:

$$V = c \cdot f_{ct} \cdot A_{cj} + \mu \cdot A_{sw} \cdot (f_y - F/A_{sw}) \quad (3)$$

where:

- c and μ are friction factors that depend on the roughness of the interface. In the considered case, being the surface a free one left without further treatment after vibration, the values of c = 0.35 and μ = 0.60 are considered;
- f_{ct} is the mean tensile strength of concrete, equal to 2.33 MPa;
- A_{sw} is the cross-section area of the stirrups crossing the joint (628 mm^2 for the sound specimen and 427 mm^2 for the damaged one);
- f_y is the mean yielding strength of rebars, equal to 530 MPa;

Calling e the distance between the forces F and T and z the distance between the forces V and C, the equilibrium to rotation about a generic point of the torn block reads:

$$V \cdot z = F \cdot e \quad (4)$$

The maximum resisting force F can be found substituting the expression of V given by (3) into (4), obtaining with some simple passages:

$$F = \frac{c \cdot f_{ct} \cdot A_{cj} \cdot z + \mu \cdot A_{sw} \cdot f_y \cdot z}{e + \mu \cdot z} \quad (5)$$

The results obtained following this verification for the sound side and the damaged side are presented in Table 3. The steel jacketing is designed in order to be able to carry 100% of the load outside of the half joint to a part of the beam able to resist (where corrosion damage is absent or small). The block tearing resistances presented in Table 3 are different for the 4 cases (orthogonal sound and damaged, inclined sound and damaged) because the amount of rebars crossing the interface between the jacketed area and non-jacketed one is different in the four cases. The plates are the same, but the reinforcing bars inside the concrete web at the end of the plates are not.

Table 3. Block tearing resistances.

	Specimen	**e [m]**	**z [m]**	**F/A_{sw} [MPa]**	**V [kN]**	**F [kN]**
Orthogonal reinforcement	Sound	0.33	0.50	355	147	**223**
	Damaged	0.38	0.50	374	121	**160**
Inclined reinforcement	Sound	0.38	0.50	346	115	**222**
	Damaged	0.41	0.50	410	100	**148**

6.2. Model for Inclined Reinforcement

In the case of inclined reinforcement, see Figure 16**b**, the only forces that are supposed to act on the jacketed block are:

- F Vertical force applied on the half joint;
- T Hanging force in the stirrups;

- F_{ih} Horizontal component of the force in the inclined reinforcements;
- F_{iv} Vertical component of the force in the inclined reinforcements;
- C. Force in the compressed chord;
- V. Shear friction resistance.

As a first approximation, in the studied beams the inclined bars pass by the lower corner of the jacketing plate and are inclined at 45°. Thanks to these conditions the equilibriums can be written in a simplified form as follows.

Horizontal equilibrium needs $V + F_{ih} = C$ and the vertical one needs $F = T + F_{iv}$.

Vertical stirrups should at least be able to carry the vertical force F, but if their section is bigger than the needed one, they can provide additional resistance in the shear friction model presented in Equation (2). The cross-section of the joint A_{cj} is the same seen for orthogonal reinforcement.

Therefore, Equation (2) can be rewritten as:

$$V = c \cdot f_{ct} \cdot A_{cj} + \mu \cdot \left(A_{sw} \cdot f_y - F + F_{iv} \right) \tag{6}$$

where A_{sw}, the cross-section area of the vertical stirrups crossing the joint, is 302 mm^2 for the sound specimen and 258 mm^2 for the damaged one, whereas the area of the inclined reinforcement is 314 mm^2 for the sound specimen and 113 mm^2 for the damaged one.

The equilibrium to rotation about the lower corner of the plate, where the forces V, F_{ih}, F_{iv} have nil lever arm, can be written as follows:

$$F \cdot e_F - T \cdot e_T - C \cdot z = 0 \tag{7}$$

that can be solved to find F

$$F = \frac{\mu \cdot A_{sw} \cdot f_y \cdot z + F_{ih} \cdot z - F_{iv} \cdot (e_T - \mu \cdot z) + c \cdot f_{ct} \cdot A_{cj} \cdot z}{\mu \cdot z + e_F - e_T} \tag{8}$$

The results obtained following this verification for the sound side and the damaged side are presented in Table 3.

7. Laboratory Tests and Numerical Simulations Result and Discussion

In this section, the authors compare the results of experimental tests to the results of numerical simulations and discuss their interpretation.

7.1. Experimental Test Results

Figure 17 shows the results of the experimental tests performed on the two beams in terms of the midspan load-displacement curve.

The behavior of the two beams in static scheme 1 (Figure 10a,b) is almost identical (continuous black and blue curves). The failure load is about 240 kN for both beams (120 kN on each half joint).

The type of collapse presents both analogies and differences: a longitudinal disconnection on the casting joint between the web and flange arises at the end of the damaged side for both beams.

The beam with orthogonal reinforcement collapses with a brittle mechanism tearing away the strengthened zone from the rest of the beam without developing a large plastic field as shown in Figure 18a,b.

In the beam with inclined reinforcement, the flange-web disconnection extends almost to the midspan leading to a more ductile behavior (see Figure 18d).

The beam with orthogonal reinforcement was tested on load scheme 2 after the failure in load scheme 1. The dashed black curve, shown in Figure 17, is relative to the test in static scheme 2, shown in Figure 10c,d. In this scheme, the sound-dapped end reaches a collapse load of about 175 kN and the collapsed end is shown in Figure 18c.

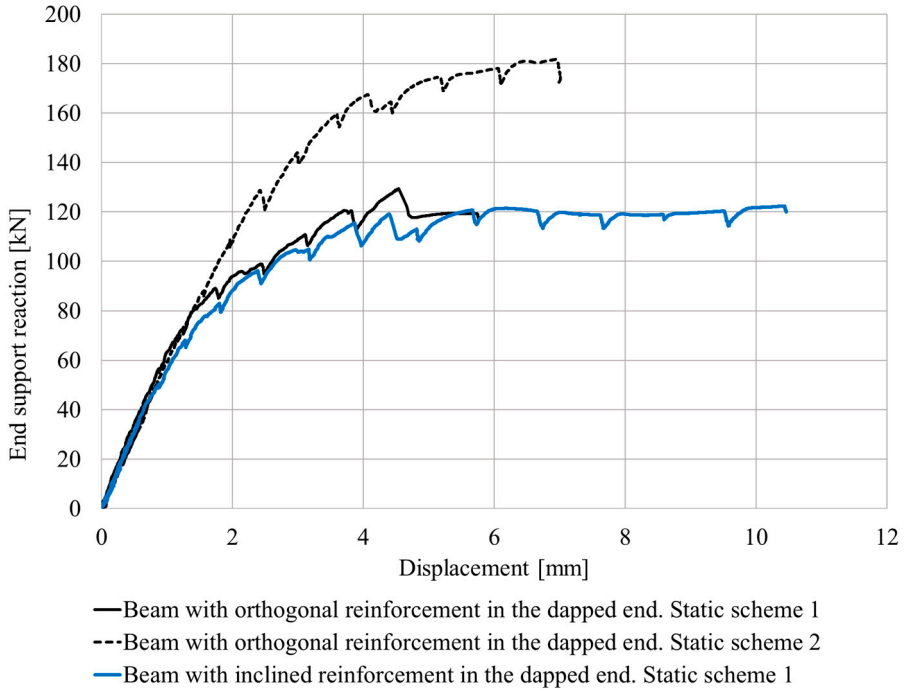

Figure 17. Laboratory test results.

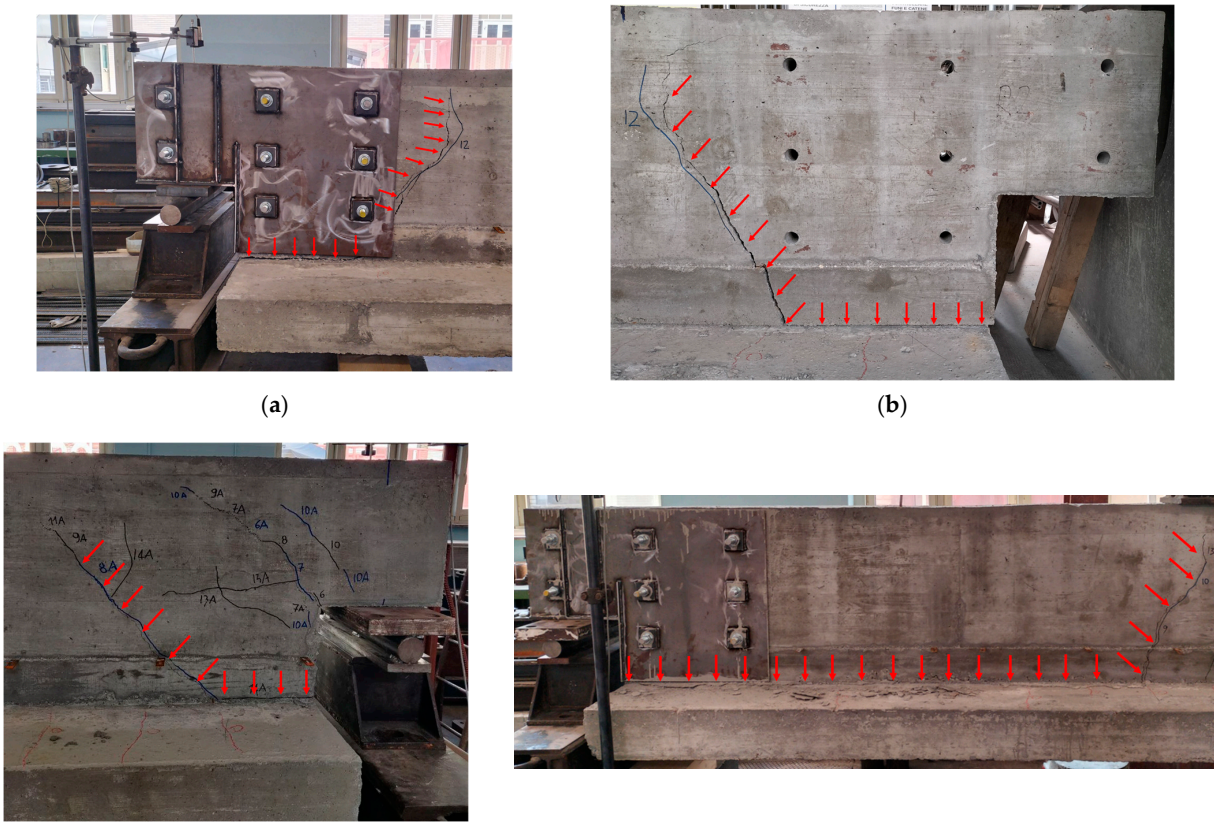

Figure 18. Collapse mechanisms. (**a**) Beam with orthogonal reinforcement in static scheme 1. (**b**) Beam with orthogonal reinforcement in static scheme 1 after removal of steel jacketing. (**c**) Beam with orthogonal reinforcement in static scheme 2. (**d**) Beam with inclined reinforcement in static scheme 1.

The beam with inclined reinforcement could not be tested in scheme 2 because the failure mechanism due to the test on static scheme 1 extends to the midspan of the beam, Figure 18d. Therefore, the beam could not be used anymore.

The collapse load calculated with STM for the sound-dapped end with orthogonal reinforcement is 150 kN. The sound side tested in the laboratory provided a resistance of 175 kN (17% higher than STM). The theoretical result is therefore in excellent agreement with the laboratory tests because STM tends to predict failure loads lower than real ones (on the safe side) being a plasticity lower bound solution.

The collapse load calculated with STM for the sound-dapped end with inclined reinforcement is 160 kN. No laboratory test can confirm this value as this beam cannot be tested in this scheme. The authors are confident that the result obtained with STM (160 kN) would also have been confirmed.

The failure loads of the damaged end without jacketing, calculated with STM, are, respectively, 65 and 70 kN for orthogonal and inclined reinforcements. The steel jacketing increased them by +85% and +72% respectively, reaching 120 kN for both reinforcements layouts. The results are shown in Table 4.

Table 4. Comparison between strut & tie (STM) and experimental results.

Beam Type	Dapped End Status	Ultimate STM Load [kN]	Ultimate Experimental Load [kN]
Orthogonal reinforcement	Sound end	150	175 (+17%)
	Damaged end	65	120 (+85%)
Inclined reinforcement	Sound end	160	[-]
	Damaged end	70	120 (+72%)

Steel jacketing, therefore, improved noteworthy the resistance of damaged ends. Nevertheless, it was not able to restore the +120% necessary to reach the sound resistance because of a failure mechanism that took place outside the jacketed area and that will be described in the following paragraph.

As can be seen in Figure 18, in both experiments no evident signs of damage is visible in the web under the jacketing plates. The strengthening system acts as a rigid block that shifts the collapse zone to the first section where the jacketing is not applied. The collapse follows the opening of a crack between the flange and the web of the T beam along the casting joint. The authors did not find in the literature any experimental test on half-joints of T beams realised in two casting phases; therefore, this study introduces two novel issues: interaction between half joint and flange of T section and the presence of flange-web construction joint.

Construction joints are an area of intrinsic weakness in the structure especially if the surface is not prepared to increase its roughness such as in this case. Real bridge beams are almost always cast in two stages, and the slab is realised a second time. Therefore, the realisation of these scaled specimens is an accurate reproduction of a real case.

Experimental evidence also shows that the application of the jacketing system evidences this weakness as the steel plates end exactly on the casting joint introducing a significant stiffness variation and concentration of stress in that zone.

The application of steel plates increases the resistance of the damaged half joint taking most of the load as no cracks are visible on the damaged dapped end after the removal of the plates at the end of the load tests. Nevertheless, it shifts the critical verification area to the interface section between the jacketed part of the beam and the not jacketed one.

7.2. Results of Numerical Simulations

The results of numerical simulations and their comparison with the results of the laboratory test are reported in this section.

Figure 19a shows the comparison between load-displacement curves of the experimental result and their FEM model of the beams tested in static scheme 1. It can be seen that orthogonal and inclined reinforcement almost have the same behaviour until yielding as it was desired from design. The numerical simulation also fairly approximates the experimental result before yielding.

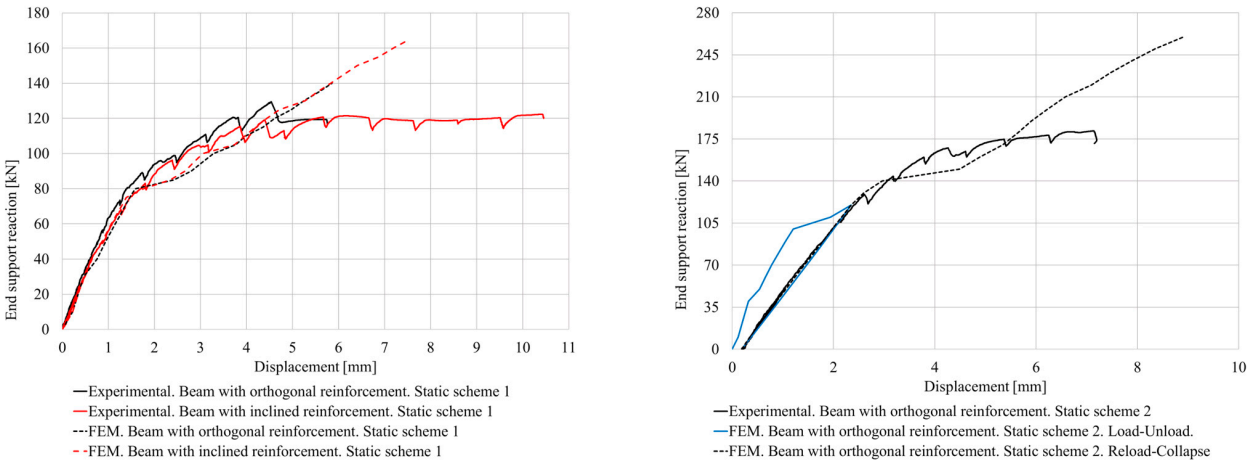

(**a**) (**b**)

Figure 19. Comparison between experimental results and numerical simulation of a beam with orthogonal reinforcement. (**a**) Static scheme 1. (**b**) Static scheme 2.

In the beam with orthogonal reinforcement, when the load of 120 kN is reached, the experimental curve shows a short plastic plateau, that corresponds to the opening of the big crack evidenced in Figure 18a,b. This plateau is not visible in the FEM model as the load increases until a collapse load is 12% higher than the experimental one.

In the beam with inclined reinforcement, when the load of 120 kN is reached, the experimental evidence shows a long plastic plateau that corresponds to the opening of the crack shown in Figure 18d. The FEM model again cannot find this plateau as the load increases until the collapse load is about 32% higher than the experimental one.

Figure 19b shows the comparison between the experimental result of the beam with orthogonal reinforcement in static scheme 2 and its FEM model. In this case, an initial load-unload phase (blue curve) was made in the FEM model to simulate the starting condition equal to the experimental one (static scheme 2 is conducted after a full load on scheme 1). Moreover, in this case, the experimental and numerical results are in good agreement in the elastic and cracking propagation phase, but the FEM model is again unable to capture the plastic field that develops due to the collapse surface evidenced in Figure 18c. The collapse load of the numerical model is about 50% higher than the experimental evidence.

In both schemes, FEM models are unable to capture the failure mechanism on the casting joint that seems to cause the collapse of the beams in reality. Different mesh sizes were tested to study the mesh dependency of the problem. A cohesive-friction interface was also introduced between the web and flange to simulate a reduction of tensile resistance without succeeding in improving the numerical solution. The numerical prediction of the failure load of concrete structures with brittle mechanisms (shear failures or D regions) is well-known in the literature [42,43]. Errors up to 30% in the prediction of the ultimate load can be achieved using commercial software and are well documented.

Figure 20 shows that the numerical crack pattern reproduces fairly well the experimental evidence in every static scheme that has been investigated. This result, in addition to the very good agreement of load-deflection curves shown in Figure 19, demonstrates the good performance of the numerical models until the sudden collapse that cannot be evidenced numerically.

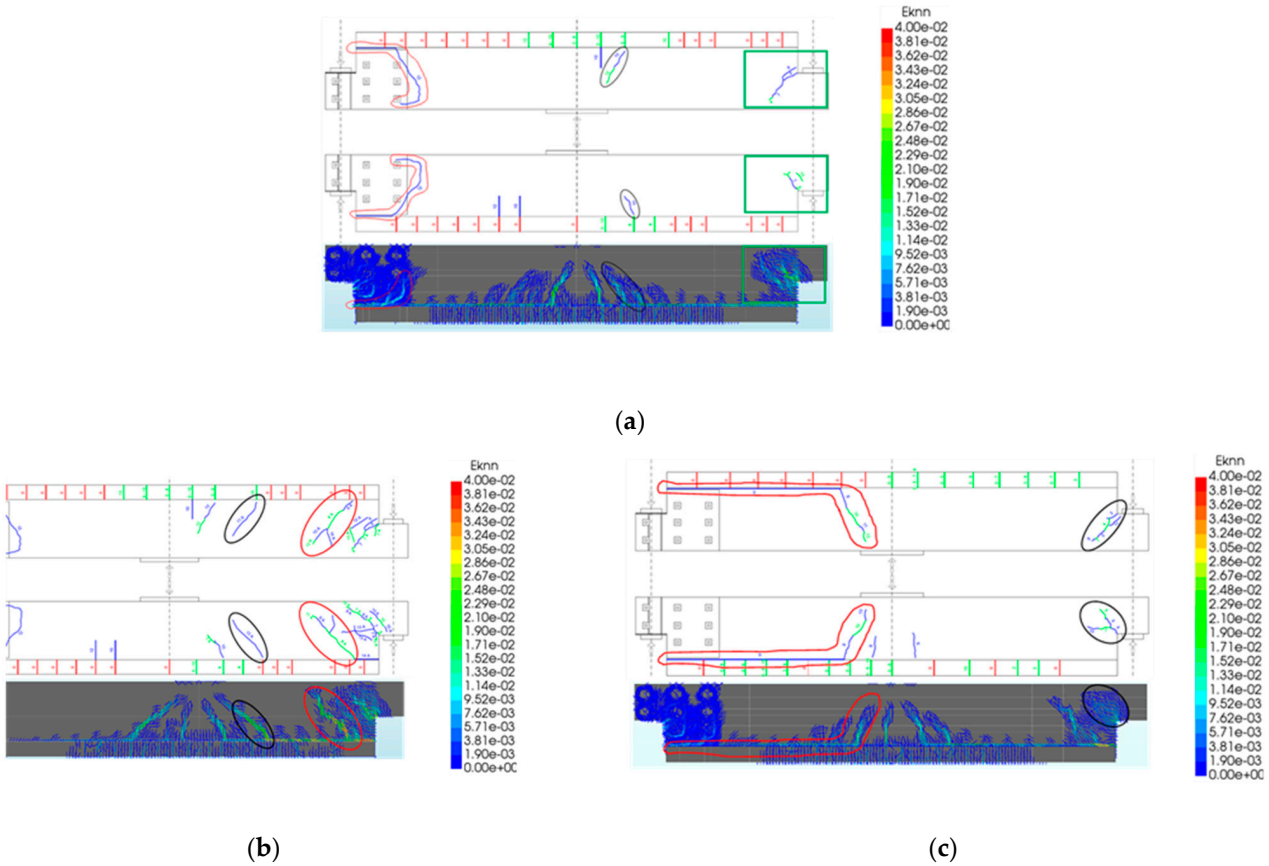

Figure 20. Comparison between experimental and numerical crack pattern. (**a**) Beam with orthogonal reinforcement in static scheme 1. (**b**) Beam with orthogonal reinforcement in static scheme 2. (**c**) Beam with inclined reinforcement in static scheme 1.

8. Final Comparison of Results

Two beams were designed, both with one sound side and one damaged side. The design was conducted both manually using analytical formulation (STM and Block tearing) and numerically, using a non-linear f.e.m. analysis.

The results are presented in Table 5. In the table, the term "Analytical" defines the minimum result obtained with STM and Block tearing models. Analytical is equal to STM where this model is applicable (sound side of the gerber saddle and damaged side without jacketing system) as the block tearing model gives higher results and is therefore excluded as not physically possible. Analytical is equal to block tearing for jacketed damaged cases.

Table 5. Comparison between failure loads [kN].

	Specimen	Experimental	Strut & Tie	Block Tearing	Analytical	f.e.m.
Orthogonal reinforcement	Sound	360	300	446	300	360
	Damaged	n.a.	130	320	130	200
	Damaged & jacketed	250	n.a.	320	320	280
Inclined reinforcement	Sound	n.a.	320	444	320	440
	Damaged	n.a.	140	296	140	220
	Damaged & jacketed	250	n.a.	296	296	330

n.a. not available.

According to the manual design, the sound sides should fail in the discontinuity region of the half joint for an applied load on the beam midspan (pier reaction) equal to

300 kN and 320 kN for straight and inclined reinforcement respectively obtained by strut & tie calculations. The same calculations provided a failure load for the damaged and not jacketed side of 130 kN and 140 kN for straight and inclined reinforcement respectively (less than 45% of sound resistance).

When jacketing is applied the strut & tie calculations are not applicable anymore and a block tearing mechanism is adopted for hand calculations of the jacketed discontinuity region. This approach provided failure loads of 320 kN and 296 kN for jacketed straight and inclined reinforcement respectively.

This result provided a theoretical failure load of the jacketed damaged side equal to one of the sound non-jacketed ones.

Laboratory tests demonstrated that both orthogonal and inclined jacketed sides failed at an applied load of 250 kN (20% less than the analytical block tearing calculation, but 85% more than the expected failure load of the damaged and unjacketed sides).

The failure registered during the experimental test was localised on the casting joint between the web and flange of the beam and did not interest the half joint area. Therefore, the failure was just outside the area covered by the jacketing system ended the tests completely undamaged.

The steel jacketing, therefore, demonstrated to be able to strongly increase the resistance of a heavily damaged half joint (+85%), but it was not able to reach the design target of +120%.

Failure was probably due to the lack of proper vertical reinforcement crossing the casting joint. This reinforcement was less than 50% of the sound side one and therefore less than the minimum one required by design code. Vertical stirrups on the damaged side were realised with a smaller diameter than the ones on the sound side; therefore, they presented a uniform cross-section reduction along their length. This choice is probably far more severe than the real corrosion effect.

Numerical design using f.e.m. provided failure loads higher than STM analytical ones for sound beams (120% and 137% respectively for orthogonal and inclined reinforcements), and higher than experimental ones for damaged jacketed beams (112% and 132% respectively for orthogonal and inclined reinforcements).

Numerical analyses provided good accordance with experimental results up to the failure loads, but they were not able to individuate the ultimate load, overestimating it in every test. Probably the brittle nature of the failure mechanism is the main reason for the difficulty in obtaining reliable numerical predictions.

Block tearing calculations also provide ultimate loads predictions higher than experimental ones for damaged jacketed beams (128% and 118% respectively for orthogonal and inclined reinforcements) probably because the shear friction formulation adopted in Equations (2) and (5) is applied with an amount of reinforcement crossing the joint smaller than the minimum one required by the design code [30].

9. Conclusions

With this work, the authors aimed to investigate an innovative strengthening system for gerber saddles. Analytical calculations, laboratory experimental tests, and numerical simulation are performed on two different beams with different reinforcement layouts in the dapped end.

A review of the state of the art showed that few studies have been conducted on the supporting part of bridge gerber saddles. Most of the studies found in the literature focus on the supported part of gerber saddles. The strengthening systems evidenced in the literature are prevalently performed with FRP/CFRP or with pretensioning systems. The first is effective for moderate levels of damage and is not highly invasive; the second is effective for more intense levels of damage but has considerable invasiveness. On this basis, the authors propose a system that should be more efficient than FRP/CFRP, but at the same time less invasive than the introduction of prestressing.

Moreover, tests on beams with strengthened dapped ends were almost exclusively conducted on beams with rectangular cross-sections: T-shaped sections with casting joints were never tested before. This aspect represents an absolute novelty point of this study.

Thus, in the present study, some significant innovations are introduced: a T-shaped beam section with the presence of a flange web casting joint; the casting of the beam in two phases; and the study of the end subjected to negative bending moment.

The beams were designed to be approximately 1:3 scale compared to the common size of real gerber saddles. The collapse load is estimated with an STM in both the undamaged and damaged dapped end.

The damaged gerber saddles were designed to support a load equal to about 45% of the sound ones. This level of damage is very high since normally in reinforced concrete decks the permanent loads exceed 50% of the total applied loads. Therefore, the designed damage would result in the collapse of the bridge under only permanent loads.

Reinforcement corrosion damage was simulated by changing the diameter of the corroded stirrups; for example, an undamaged stirrup Φ8 or Φ10 was replaced with a damaged stirrup Φ6. This operation uniformly reduced the area of the stirrups whereas in real conditions corrosion is more concentrated in the part of the stirrup within the half joint as it is more exposed to water leakages.

The authors decided to simulate corrosion with diameter change because of the scheduling of the financed research that did not allow the use of accelerated corrosion techniques.

Web stirrups almost always maintain their original area at the connection with the beam flange (in the casting joint).

The application of the steel strengthening failed to raise the strength of the damaged dapped end to the level of the undamaged ones, as it was intended, but the collapse load still increased from about 45% to about 80% percent of the value of the undamaged dapped end. The strengthening system thus proved to be able to increase the strength of the gerber saddle in a nonnegligible way.

Both laboratory specimens collapsed with a similar failure mechanism involving a longitudinal crack dividing the web from the flange of the beams.

The weakness of the shear-friction resistance of the joint between the web and flange may be a collateral effect of the stirrups damage simulation mode and should not be probable in real operating conditions.

The authors believe that the "block tearing" collapse mechanism seen in the experimental tests needs to be furtherly investigated to understand whether this mechanism is only due to the low amount of stirrups crossing the casting joint, or if the steel jacketing causes its initiation.

From the experimental tests, hand calculations and numerical calculations performed, the following considerations can be made:

- Both strengthened gerber saddles reached collapse by a similar mechanism involving the failure of the casting joint and a shear crack in the web with an inclination of about 60°. This phenomenon had never been studied in the literature in conjunction with the behavior of gerber saddles.
- This mechanism may have been promoted by three causes:
  a. the stirrups crossing the casting joint were weakened to simulate corrosion even in an area where they are not normally corroded;
  b. the surface of the casting joint was not prepared to increase its roughness and promote interlock between castings;
  c. the presence of the steel jacketing may have concentrated stresses on the casting joint, although there is currently no numerical evidence of this phenomenon.
- The steel plates and bolts remained in the elastic field and resisted correctly. The purely "steel" part of the jacketing behaved properly.
- The friction interface between steel plates and the web of the beam resisted correctly and did not slip, even though there was no grout between the plates and the web

and the surface of the web was not prepared and it was irregular due to the wooden formwork.
- The strength of the only undamaged gerber tested was correctly prognosticated by manual calculations with STM.
- On the contrary, the strength of both naked and jacketed sides was lower than the one obtained by numerical simulations. The numerical models provided good accordance until the failure load, but they were not able to catch the failing mechanism correctly.

A new testing campaign with a better simulation of real corrosion conditions should be performed in order to investigate if the casting joint failure can be avoided and the full potential of the jacketing system can be exploited.

Author Contributions: Conceptualization, G.B. and L.G.; methodology, M.F. and G.B.; software, M.F.; validation, M.F., L.G. and M.M.; formal analysis, M.F.; investigation, M.F.; resources, M.M.; data curation, M.F. and G.B.; writing—original draft preparation, M.F. and G.B.; writing—review and editing L.G., G.B.; visualization, M.F.; supervision G.B.; project administration, G.B. and L.G.; funding acquisition, G.B., L.G. and M.M. All authors have read and agreed to the published version of the manuscript.

Funding: This research was funded within the framework of "Argo Innovation Lab" project, promoted by Elis Innovation Hub and Movyon S.p.A.

Institutional Review Board Statement: Not applicable.

Informed Consent Statement: Not applicable.

Data Availability Statement: The data presented in this study are available on request from the corresponding author.

Conflicts of Interest: The authors declare no conflict of interest.

References

1. Neves, L.C.; Frangopol, D.M. Condition, safety and cost profiles for deteriorating structures with emphasis on bridges. *Reliab. Eng. Syst. Saf.* **2005**, *89*, 185–198. [CrossRef]
2. Ministero delle Infrastrutture e della Mobilità Sostenibili. *Linee Guida per la Classificazione e Gestione del Rischio, la Valutazione Della Sicurezza ed il Monitoraggio dei Ponti Esistenti*; Decreto 01-07-2022; Ministero delle Infrastrutture e della Mobilità Sostenibili: Rome, Italy, 2022.
3. Cosenza, E.; Losanno, D. Assessment of existing reinforced-concrete bridges under road-traffic loads according to the new Italian guidelines. *Struct. Concr.* **2021**, *22*, 2868–2881. [CrossRef]
4. Miluccio, G.; Losanno, D.; Parisi, F.; Cosenza, E. Fragility analysis of existing prestressed concrete bridges under traffic loads according to new Italian guidelines. *Struct. Concr.* **2023**, *24*, 1053–1069. [CrossRef]
5. Cosenza, E.; Losanno, D. A focus on the new Italian guidelines for safety assessment of existing bridges (Key-note lecture). In Proceedings of the 2nd Workshop on Capacity Assessment of Corroded Reinforced Concrete Structures, CACRCS DAYS 2020, online, 1–4 December 2020.
6. Lee, D.J. *Bridge Bearings and Expansion Joints*, 2nd ed.; CRC Press: Boca Raton, FL, USA, 1995. [CrossRef]
7. Di Prisco, M.; Colombo, M.; Martinelli, P.; Coronelli, D. The technical causes of the collapse of Annone overpass on SS.36. In Proceedings of the Italian Concrete Days Aicap and CTE, Milan/Lecco, Italy, 13–16 June 2018.
8. Spinella, N.; Messina, D. Load-bearing capacity of Gerber saddles in existing bridge girders by different levels of numerical analysis. *Struct. Concr.* **2023**, *24*, 211–226. [CrossRef]
9. Di Carlo, F.; Meda, A.; Molaioni, F.; Rinaldi, Z. Experimental evaluation of the corrosion influence on the structural response of Gerber half-joints. *Eng. Struct.* **2023**, *285*, 116052. [CrossRef]
10. Santarsiero, G.; Picciano, V. Durability enhancement of half-joints in RC bridges through external prestressed tendons: The Musmeci Bridge's case study. *Case Stud. Constr. Mater.* **2023**, *18*, e01813. [CrossRef]
11. Granata, M.F.; La Mendola, L.; Messina, D.; Recupero, A. Assessment and strengthening of reinforced concrete bridges with half-joint deterioration. *Struct. Concr.* **2023**, *24*, 269–287. [CrossRef]
12. Huang, P.-C.; Nanni, A. Dapped-End Strengthening of Full-Scale Prestressed Double Tee Beam with FRP Composite. *Adv. Struct. Eng.* **2006**, *9*, 293–308. [CrossRef]
13. Taher, F. Strengthening o critically designed girders with dapped ends. *Struct. Build.* **2005**, *158*, 141–152. [CrossRef]
14. Atta, A.; Taman, M. Innovative method for strengthening dapped-end beams using an external prestressing technique. *Mater. Struct.* **2016**, *49*, 3005–3019. [CrossRef]
15. Mattock, A.H.; Chan, T.C. Design and Behavior of Dapped-End Beams. *PCI J.* **1979**, *24*, 28–45. [CrossRef]

16. Mattock, A.H. Design proposal for reinforced concrete corbels. *PCI J.* **1976**, *21*, 18–42. [CrossRef]
17. Liem, S.K. Maximum Shear Strength of Dapped-End or Corbel. Master's Thesis, Concordia University, Montreal, QC, Canada, 1983.
18. Barton, D.L.; Anderson, R.B.; Bouardi, A.; Jirsa, J.O.; Breen, J.E. *An Investigation of Strut-and-Tie Models for Dapped Beam Details*; Research Report Number 1127-1; Texas State Department of Highways and Public Transportation: Austin, TX, USA, 1991.
19. Desnerck, P.; Lees, J.M.; Morley, C.T. Strut-and-tie models for deteriorated reinforced concrete half-joints. *Eng. Struct.* **2018**, *161*, 41–54. [CrossRef]
20. Mata-Falcón, J.; Pallarés, L.; Miguel, P.F. Proposal and experimental validation of simplified strut-and-tie models on dapped-end beams. *Eng. Struct.* **2019**, *183*, 594–609. [CrossRef]
21. Desnerck, P.; Lees, J.M.; Morley, C.T. Impact of the reinforcement layout on the load capacity of reinforced concrete half-joints. *Eng. Struct.* **2016**, *127*, 227–239. [CrossRef]
22. Desnerck, P.; Lees, J.M.; Morley, C.T. The effect of local reinforcing bar reductions and anchorage zone cracking on the load capacity of RC half-joints. *Eng. Struct.* **2017**, *152*, 865–877. [CrossRef]
23. Aswin, M.; Al-Fakih, A.; Syed, Z.I.; Liew, M.S. Influence of Different Dapped-End Reinforcement Configurations on Structural Behavior of RC Dapped-End Beam. *Buildings* **2023**, *13*, 116. [CrossRef]
24. Nagy-György, T.; Sas, G.; Dăescu, A.C.; Barros, J.A.O.; Stoian, V. Experimental and numerical assessment of the effectiveness of FRP-based strengthening configurations for dapped-end RC beams. *Eng. Struct.* **2012**, *44*, 291–303. [CrossRef]
25. Quadri, A.I. Behavior of disturbed region of RC precast beams upgraded with near surface mounted CFRP fiber. *Asian J. Civ. Eng.* **2023**, *24*, 1859–1873. [CrossRef]
26. Sas, G.; Dăescu, C.; Popescu, C.; Nagy-György, T. Numerical optimization of strengthening disturbed regions of dapped-end beams using NSM and EBR CFRP. *Compos. Part B Eng.* **2014**, *67*, 381–390. [CrossRef]
27. Abdel-Moniem, A.; Madkour, H.; Farah, K.; Abdullah, A. Numerical Investigation for external Strengthening of Dapped-End Beams. *Int. J. Archit. Civ. Constr. Sci.* **2018**, *12*, 1474911.
28. Baraghith, A.T.; Khalil, A.H.A.; Etman, E.E.; Behiry, R.N. Improving the shear behavior of RC dapped-end beams using precast strain-hardening cementitious composite (P-SHCC) plates. *Structures* **2023**, *50*, 978–997. [CrossRef]
29. Atta, A.M.; El-Shafiey, T.F. Strengthening of RC dapped-end beams under torsional moment. *Mag. Concr. Res.* **2014**, *66*, 1065–1072. [CrossRef]
30. *EN 1992-1-1*; Eurocode 2: Design of Concrete Structures. European Committee for Standardization (CEN): Brussels, Belgium, 2004.
31. Giordano, L.; Mancini, G.; Tondolo, F. Reinforced Concrete Members Subjected to Cyclic Tension and Corrosion. *J. Adv. Concr. Technol.* **2011**, *9*, 277–285. [CrossRef]
32. Bico, F.; Bartoli, M.; Di Carlo, F.; Meda, A.; Molaioni, F.; Rinaldi, Z. Structural behavior of PC beams under simultaneous corrosion and sustained loads. In *Life-Cycle of Structures and Infrastructure Systems, Proceedings of the IALCCE 2023 Eight International Symposium on Life-Cycle Civil Engineering, Milan, Italy, 6 July 2023*; Biondini, F., Frangopol, D.M., Eds.; Amer Society of Civil Engineers: New York, NY, USA, 2023.
33. *EN1993-1-8*; Eurocode 3: Design of Steel Structures—Design of Joints. European Committee for Standardization (CEN): Brussels, Belgium, 2005.
34. *Theory Manual of DIANA FEA*; Release 10.2; DIANA FEA BV: Delft, The Netherlands, 2016.
35. *Element Library of DIANA FEA*; Release 10.2; DIANA FEA BV: Delft, The Netherlands, 2016.
36. Cervera, M.; Chiumenti, M. Smeared crack approach: Back to the original track. *Int. J. Numer. Anal. Meth. Geomech.* **2006**, *30*, 1173–1199. [CrossRef]
37. Vecchio, F.J.; Collins, M.P. The modified compression field theory for reinforced concrete elements subjected to shear. *ACI J.* **1986**, *83*, 219–231.
38. Selby, R.G.; Vecchio, F.J. *Three-Dimensional Constitutive Relations for Reinforced Concrete*; University of Toronto, Department of Civil Engineering: Toronto, ON, Canada, 1993.
39. Vecchio, F.J.; Collins, M.P. Compression response of cracked reinforced concrete. *J. Str. Eng. ASCE* **1993**, *119*, 3590–3610. [CrossRef]
40. Selby, R.G.; Vecchio, F.J. A constitutive model for analysis of reinforced concrete solids. *Can. J. Civ. Eng.* **1997**, *24*, 460–470. [CrossRef]
41. *Material Library of DIANA FEA*; Release 10.2; DIANA FEA BV: Delft, The Netherlands, 2017.
42. Belletti, B.; Damoni, C.; Hendriks, M. Non-Linear Finite Element Analyses of Existing Reinforced Concrete Bridge Beams. In *Assessment, Upgrading and Refurbishment of Infrastructures, Proceedings of the IABSE Conference: Assessment, Upgrading and Refurbishment of Infrastructures, Rotterdam, The Netherlands, 6–8 May 2013*; IABSE: Zurich, Switzerland, 2013; pp. 520–521.
43. Castaldo, P.; Gino, D.; Bertagnoli, G.; Mancini, G. Partial safety factor for resistance model uncertainties in 2D non-linear finite element analysis of reinforced concrete structures. *Eng. Struct.* **2018**, *176*, 746–762, ISSN 0141-0296. [CrossRef]